High Power Laser Science and Engineering, (2025), Vol. 13, e98, 8 pages.
doi:10.1017/hpl.2025.10088

RESEARCH ARTICLE

All-fiber high-power tunable dual-pulse laser with ps/ns pulse width

Chaojian He[1,2,3,4], Haijuan Yu[1,2,3,4], Xinyao Li[1], Wenjuan Wu[1,2,3,4], Shuzhen Zou[1,4], Song Yang[1,2,3,4], and Xuechun Lin[1,2,3,4]

[1]*Laboratory of All-Solid-State Light Sources, Institute of Semiconductors, Chinese Academy of Sciences, Beijing, China*

[2]*College of Materials Science and Opto-Electronic Technology, University of Chinese Academy of Sciences, Beijing, China*

[3]*Center of Materials Science and Optoelectronics Engineering, University of Chinese Academy of Sciences, Beijing, China*

[4]*Beijing Engineering Technology Research Center of All-Solid-State Lasers Advanced Manufacturing, Beijing, China*

(Received 12 August 2025; revised 29 September 2025; accepted 29 October 2025)

Abstract

We demonstrate a high-power, flexibly tunable dual-pulse laser via temporal modulation techniques to overcome conventional systems' fixed pulse width and temporal interval constraints, enhancing precision micro/nanofabrication and nonlinear photonics applications. By combining dispersion-engineered seed pulse shaping for adjustable pulse widths (5.6 ps and 0.38–0.47 ns) with optical-delay synchronized interval tuning (from –4 to 12.5 ns), the system achieves wide flexibility in pulse configuration. Furthermore, detailed nonlinear dynamics studies reveal the picosecond component exhibits reduced amplifier efficiency versus the nanosecond component, primarily due to peak-power-driven irreversible energy transfer to Raman-shifted wavelengths. This unique combination of features enables remarkable performance: 1092 W average power at 16 MHz with precisely tailored 15.9 ps/0.44 ns pulse widths and 4.2 ns temporal interval. This high-power tunability establishes a transformative material processing paradigm from precision machining to photonics, advancing fundamental nonlinear pulse science and setting new industrial laser standards.

Keywords: fiber amplifier; fiber laser; high power; tunable dual-pulse laser

1. Introduction

Dual-pulse lasers (DPLs) with vastly different pulse widths, especially integrating femtosecond (fs) or picosecond (ps) ultra-short pulses (USPs) with nanosecond (ns) pulses (NPs), exhibit superior acquisition rates, spectral resolution and signal-to-noise characteristics in spectroscopic and metrological applications[1–5]. Furthermore, the unique ability to simultaneously exploit both non-thermal ('cold') and thermal ('hot') processing mechanisms facilitates transformative advances in applications such as laser-induced breakdown spectroscopy and high-precision material processing, leading to improvements in spatial resolution and a reduction in detection thresholds[6,7]. Thus, the DPL, as a pioneering technological platform, can effectively bridge the realms of ultrafast photonics and high-intensity material interactions[8]. Generally, the realization of DPLs relies on two fundamental approaches: intrinsic dual-pulse generation within a single laser cavity and external synchronization of parallel two-laser systems[6,9,10].

DPL generation within a single laser cavity has been extensively studied, primarily via three approaches: temporal multiplexing, spatial multiplexing and polarization multiplexing[9–12]. For instance, two laser beams generated from a bidirectional configuration exhibit output powers of 50 and 72 mW at 45.9 MHz, but with a 140 Hz repetition rate offset[10]. The polarization-multiplexed dual-pulse mode-locked fiber laser also achieved pulse widths of 1.53 and 1.47 ps, respectively, and repetition rate differences in the range of 110–250 Hz[13]. However, these kinds of fiber-based DPL systems face critical limitations: (1) restricted pulse width tunability, confined to fs-to-ps pulse widths; (2) limited temporal separation capabilities, typically operating at the ps level; and (3) significant nonlinearity constraints, as soliton mode-locked fiber lasers inherently suffer from excessive nonlinear phase accumulation[9,14].

In solid-state lasers, DPLs have been demonstrated using spatial and polarization multiplexing techniques, achieving

Correspondence to: X. Lin and H. Yu, Laboratory of All-Solid-State Light Sources, Institute of Semiconductors, Chinese Academy of Sciences, Beijing 100083, China. Emails: xclin@semi.ac.cn (X. Lin); hjyu@semi.ac.cn (H. Yu)

© The Author(s), 2025. Published by Cambridge University Press in association with Chinese Laser Press. This is an Open Access article, distributed under the terms of the Creative Commons Attribution-NonCommercial licence (https://creativecommons.org/licenses/by-nc/4.0), which permits non-commercial re-use, distribution, and reproduction in any medium, provided the original article is properly cited. The written permission of Cambridge University Press or the rights holder(s) must be obtained prior to any commercial use.

https://doi.org/10.1017/hpl.2025.10088 Published online by Cambridge University Press

MHz repetition rates and watt-level output powers[15–19]. For instance, spatial multiplexing has enabled dual-pulse mode-locking at 80 MHz, yielding a single-beam power exceeding 2.4 W with pulse widths below 140 fs[18]. Separately, polarization splitting in thin-disk lasers generates asynchronous pulse trains with pulse widths of 240 fs, average powers of 6 and 8 W per train and repetition rates of 97 MHz at 1030 nm[19]. Despite these advances, such implementations typically produce fs or ps dual pulses with fixed, small temporal separations dictated by optical path difference, while suffering from limited pulse energy and inflexible power ratio control. These constraints – particularly the inability to independently adjust pulse parameters – significantly restrict their applicability in precision laser machining.

In external synchronization of parallel laser systems, the current industrial-standard parallel dual-laser configuration provides independent parameter control but suffers from inherent timing jitter, beam divergence and system complexity[6]. Consequently, these limitations highlight the critical need for innovative approaches to achieve high-power, tunable dual pulse with ps/ns pulse widths generation based on a single cavity.

To address these issues, this study presents a DPL generation scheme based on independent temporal modulation, which enables a flexible tunable pulse width and temporal interval. Through time-domain stretching of the broadband seed pulses, synchronous DPLs with pulse widths of 5.6 ps and 0.42 ns are successfully achieved based on a single cavity. Precision control of temporal intervals is achieved via optical-delay adjustment, providing ps-level synchronization accuracy, from –4 to 12.5 ns. Employing an acoustic optical modulator (AOM), continuous tuning of repetition rates across a wide range from 100 kHz to 32 MHz is realized. Furthermore, a master oscillator power amplifier (MOPA) validated system demonstrates a maximum output power of 1092 W (16 MHz), producing 15.9 ps and 0.44 ns pulses – establishing a high-power DPL source. The proposed single-cavity based DPL generation scheme overcomes traditional limits, enabling synergistic USP/NP interactions while solving DPL synchronization/complexity issues for precision applications.

2. Experiment setup

The high-power all-fiber DPL system, as shown in Figure 1, comprises three principal parts: a passively mode-locked seed source, a DPL generator and a main amplifier. The seed source consists of a 300-mW 976 nm laser diode (LD), a wavelength division multiplexer (WDM), a semiconductor saturable absorber mirror (SESAM), a piece of 0.5 m Yb^{3+}-doped single-mode fiber and a 1064 nm fiber Bragg grating (FBG) with 30% reflectivity and –3 dB spectral bandwidth of 1 nm.

The seed pulse is then injected into the DPL generator. In particular, it first passes through a pre-amplifier (PAM1) for power enhancement and then is divided into two beams via a fused coupler (FC1). One beam is temporally broadened first owing to a tunable pulse stretcher (TPSR) and then propagates though a power attenuator (PA). The TPSR is a compact, robust and cost-effective chirped fiber Bragg grating (CFBG) to control pulse durations. Another beam propagates through an optical-delay line (ODL) and another PA. Then, the two beams are coupled into one though the 2×2 FC2, amplified by PAM2. The repetition rate of the DPL is controlled by an AOM and an arbitrary waveform generator (AWG).

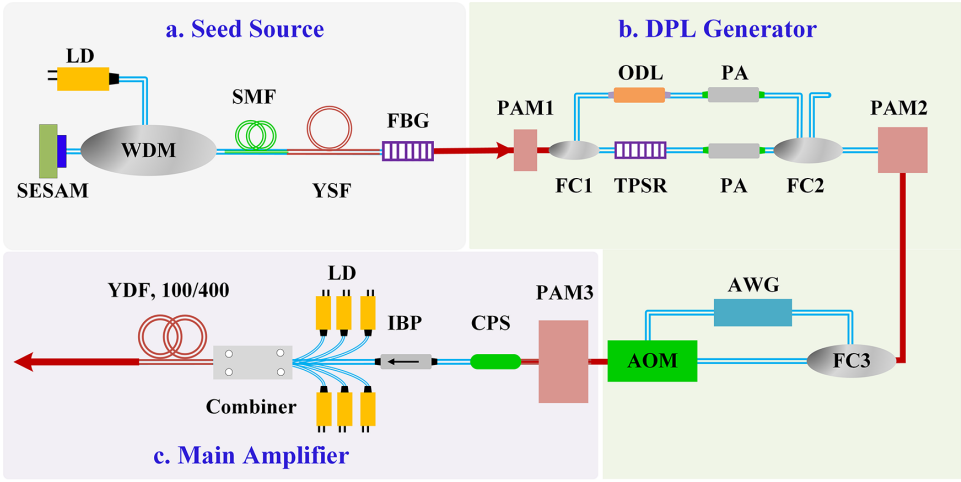


Figure 1. Schematic of the high-power DPL. LD, laser diode; YSF, Yb^{3+}-doped single-mode fiber; SMF, single-mode fiber; SESAM, semiconductor saturable absorber mirror; FBG, fiber Bragg grating; WDM, wavelength division multiplexer; PAM, pre-amplifier; FC, fused coupler; ODL, optical-delay line; PA, power attenuator; TPSR, tunable pulse stretcher (PowerSpectrum™ TPSR, TeraXion); AOM, acousto-optic modulator; AWG, arbitrary waveform generator; CPS, cladding power stripper; IBP, isolator with a bandpass filter; YDF, Yb^{3+}-doped fiber.

https://doi.org/10.1017/hpl.2025.10088 Published online by Cambridge University Press

The main amplifier comprises PAM3 and a multi-mode amplifier that consists of a 4 m extra-large-mode-area 100/400 μm Yb^{3+}-doped fiber, six 300 W 976 nm LDs and a (6 + 1) × 1 multi-mode pump/signal combiner. A cladding power stripper (CPS) is used after the pre-amplifier stage to strip residual pump light, while an isolator with a bandpass filter (IBP) is placed between stages to isolate back-reflected light and filter out amplified spontaneous emission (ASE) from the preceding stage, ensuring spectral purity for the next amplification stage. All optical components are mounted on water-cooled heat sinks to maintain thermal stability.

The pulse sequence in our experiment is measured with a 5 GHz bandwidth photodetector (Thorlabs, DET08CL), a 4 GHz bandwidth oscilloscope (Agilent Technologies, DSO7104B), an autocorrelator (APE, SM-2000) and a spectrometer (Yokogawa, AQ6370D).

3. Results and discussion

3.1. Tunable DPL

To achieve DPL operation in the USP and NP, a mode-locked fiber oscillator is designed as shown in Figure 1(a). The maximum output power of the mode-locked pulse is 3.2 mW with a repetition rate of 32 MHz. The –3 dB bandwidth $\Delta\lambda_{pulse}$ and the pulse width, as shown in Figures 2(a) and 2(b), are 0.64 nm and 5.6 ps, respectively, confirming USP generation.

Since the generation of the ps/ns DPL relies on first generating the NP, the next step is to generate the NP. As shown Figure 1(b), the USP passes through the 1×2 FC1 with a splitting ratio of 4:6, with 60% of the power coupled into the TPSR for temporal broadening. However, an insertion loss can also be introduced by the TPSR. Therefore, PAM1 is introduced before FC1 to enhance the power and compensate for the loss. The amplified pulse, as shown in Figure 2(c), demonstrates a –3 dB bandwidth of 0.72 nm under 10 mW output power.

The temporal broadening $\Delta\tau_{total}$ induced by the TPSR can be expressed as follows:

$$\Delta\tau_{total} \approx \mathrm{GVD} \cdot \Delta\lambda_{pulse},$$

where GVD is the group velocity dispersion introduced by the TPSR and $\Delta\lambda_{pulse}$ is the input pulse bandwidth[20]. In our experiment, the GVD can be continuously adjusted between 500 and 720 ps/nm.

In particular, when the GVD is set to 500, 600 and 650 ps/nm, the corresponding stretched pulse widths are 0.38, 0.42 and 0.47 ns, respectively, as shown in Figures 3(a)–3(c). It can be seen that this dispersion enables controlled temporal broadening of the USP while nearly preserving its temporal profile. Further increasing the GVD to 720 ps/nm results in pulse broadening to 0.53 ns, as shown in Figure 3(d). However, pulse splitting is also observed, demonstrating a deterioration in the pulse temporal profile. To maintain the single-pulse operation, the stretched pulse with duration of 0.42 ns at GVD = 600 ps/nm is adopted for the subsequent amplification. Subsequently, the USP and the NP are combined using a 2×2 FC, generating a DPL sequence.

The temporal interval is another important factor for improving the accuracy in the laser processing applications. Thus, except for the pulse width difference, the adjustment of the temporal interval between the two pulses is also desired. Meanwhile, the tunable temporal interval is primarily achieved by changing the optical path difference between the NP and USP sequences, as shown in Figure 1(b). In particular, an ODL (1.2 ns with 1 ps adjustment accuracy) is inserted into the USP path. Coarse adjustment of the temporal interval, typically with ns precision, is accomplished by varying the fiber length, while fine-tuning at the ps-level resolution is achieved via the ODL. This dual-adjustment mechanism enables a broad range of temporal interval modulation with a high resolution. The maximum tunable temporal interval ranges from –15.6 to +15.6 ns, which is determined by the pulse interval of the seed source.

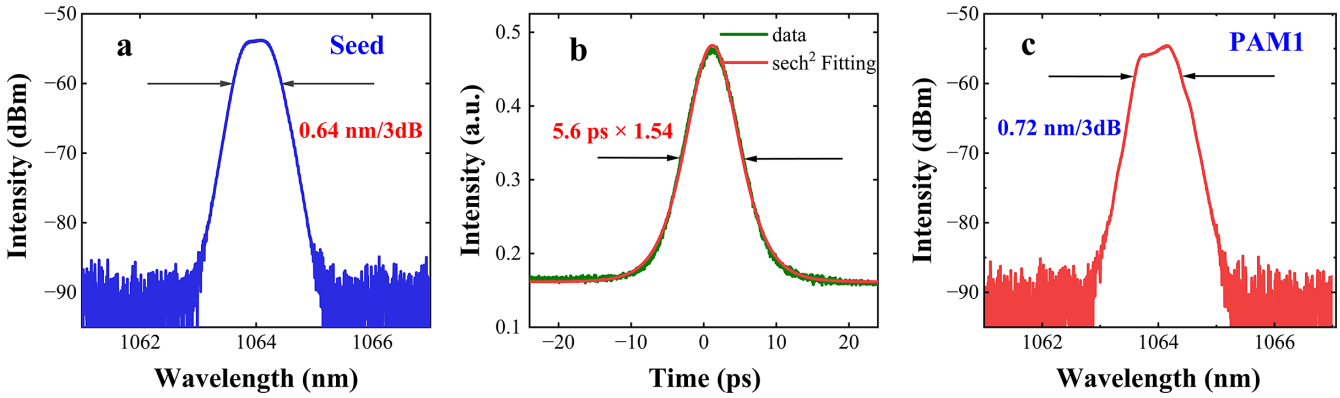


Figure 2. (a) Optical spectrum and (b) autocorrelation trace of the mode-locked seed pulse. (c) Optical spectrum of the laser pulse after PAM1.

https://doi.org/10.1017/hpl.2025.10088 Published online by Cambridge University Press

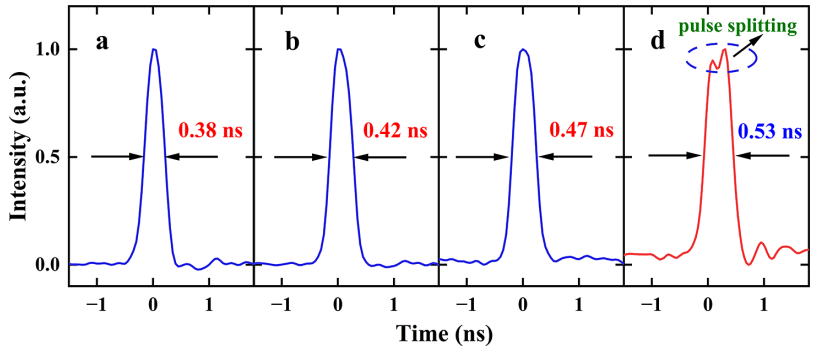


Figure 3. Typical pulse widths of the USP with (a) 500, (b) 600, (c) 650 and (d) 720 ps/nm GVD introduced by the TPSR.

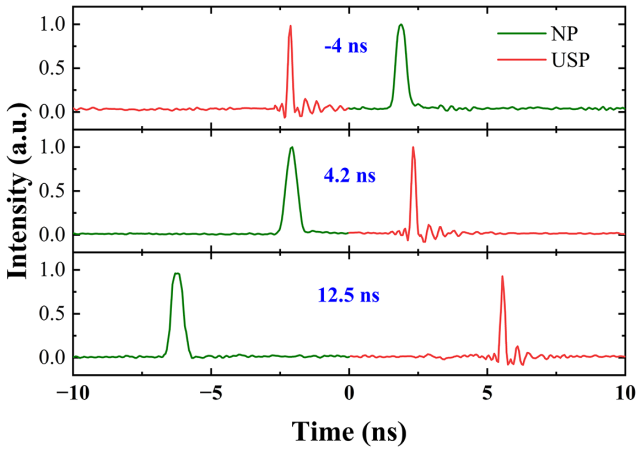


Figure 4. DPLs with temporal intervals of –4, 4.2 and 12.5 ns, respectively.

The positive value indicates that the NP precedes the USP, whereas a negative value signifies that the USP leads the NP. The temporal interval range cannot be further enlarged constrained by the repetition rate of the seed source. Figure 4(a) shows temporal profiles of the dual-pulse structure with intervals of –4, 4.2 and 12.5 ns, illustrating the feasibility of flexible control. Furthermore, the repetition rate of the DPL can be tuned from 100 kHz to 32 MHz by varying the settings of the AWG.

In practical applications, active control of the inter-pulse power ratio is essential, since their divergent nonlinear responses induce efficiency variations in energy extraction, mandating individualized pulse optimization[21]. By adjusting the PA, precise control of the dual-pulse power ratio is achieved while simultaneously enabling the generation of fixed pulse width pulses. Furthermore, independent adjustments of the ODL and PA allow the precise and flexible modulation of both the temporal interval and power ratio. Thus, it can be seen from the above results that the proposed configuration enables the realization of an all-fiber DPL featuring four key tunable characteristics: (1) pulse widths; (2) temporal intervals; (3) power ratios; (4) repetition rates. Notably, since both pulse trains originate from the same seed laser, the system maintains intrinsic coherence without an additional passive synchronous control device. This integrated architecture makes it particularly suitable for subsequent amplification, while serving as a versatile optical source for various applications requiring tailored DPL outputs.

3.2. *Main amplifier*

Applications such as nano/micro fabrication demand high-power lasers to meet rigorous processing requirements[22–25]. Thus, in this part, the amplification properties of the proposed DPL are investigated. A seed source operating at 32 MHz with an average power of 307 mW has been chosen for subsequent pulse selection and amplification. The power ratio of a DPL output, with 12.9 ps and 0.43 ns pulse widths separated by 4.2 ns temporal intervals, is approximately 1:1 and is preserved for subsequent amplification studies. Figure 5 presents the temporal profile and amplified spectrum of the DPL. The signal-to-noise ratio (SNR) of the DPL is 38.3 dB, as shown in Figure 5(b). After the two pulses are coupled, PAM3 is cascaded with a multi-mode fiber amplifier to provide amplification. After PAM3, the powers of the DPL are quantified as follows: 5.13 W at 16 MHz, 4.96 W at 6.4 MHz and 4.79 W at 3.2 MHz.

Figure 6 presents amplified powers and corresponding spectra for DPL operation, NP operation and USP operation, at a repetition rate of 16 MHz. The DPL (blue line) achieves a maximum output power of 1092 W with an optical-to-optical conversion efficiency (η) of 80%. Similarly, the NP (green line) reaches a maximum output power of 1148 W at η = 84.1%. In contrast, the USP (red line) delivers a comparatively low maximum output power of 412 W, with a conversion efficiency of 63.4%. This limitation is mainly due to the onset of pulse instabilities at high pump power levels, which can lead to detrimental effects, including irreversible optical fiber damage.

Comparative analysis reveals significant divergence in amplification characteristics across pulse duration regimes. The USP exhibits efficiency saturation when pulse energy exceeds 7.75 μJ (124 W@16 MHz), manifested as progressively decreasing amplification efficiency. In

https://doi.org/10.1017/hpl.2025.10088 Published online by Cambridge University Press

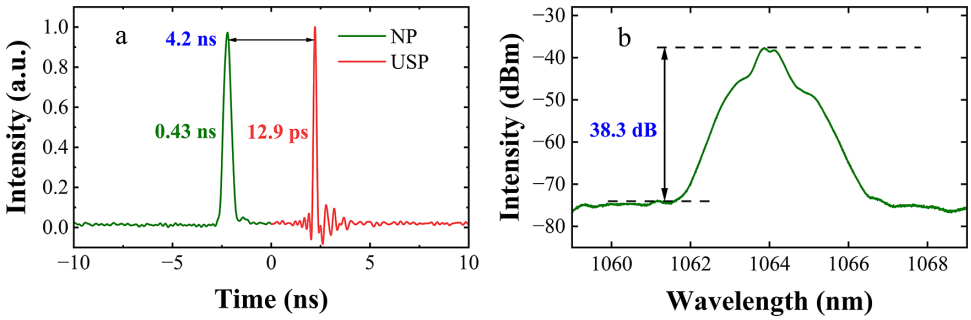


Figure 5. (a) The temporal profile and (b) the corresponding spectrum of the DPL.

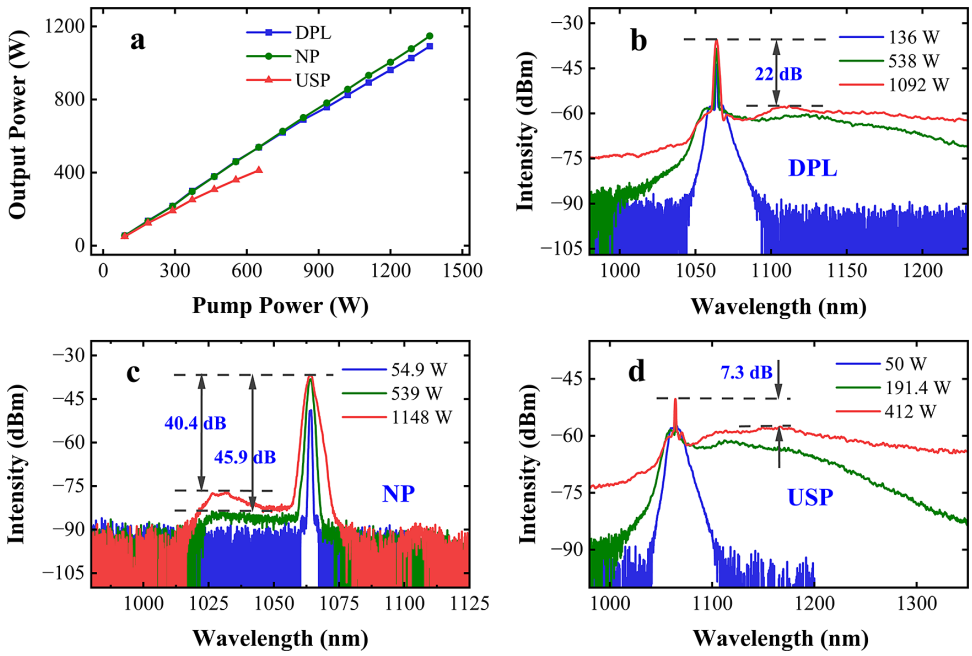


Figure 6. (a) The output power of the main amplifier versus pump power under DPL, NP and USP operations. (b) Spectra of DPL operation under 136, 538 and 1092 W output. (c) Spectra of NP operation under 54.9, 539 and 1148 W output. (d) Spectra of USP operation under 50, 191.4 and 412 W output.

contrast, both NP and DPL operations maintain linear power scaling behavior. Notably, when DPL pulse energy exceeds 38.75 μJ (620 W@16 MHz), the DPL exhibits reduced amplification efficiency compared to the NP, which may be due to the influence of the USP of the DPL. A comparative spectral analysis of the amplified pulses is conducted to elucidate the underlying physical mechanisms.

Figures 6(b)–6(d) systematically investigate the spectral evolution in the main amplifier under three different operations. Notably, Figure 6(b) reveals severe spectral broadening under DPL operation at 1092 W, primarily driven by strong nonlinear effects, particularly stimulated Raman scattering (SRS). The SNR decreases to only about 22 dB. In contrast, Figure 6(c) demonstrates that the NP operation maintains an exceptional SNR of 40.4 dB even at a higher power of 1148 W, while ASE dominates the noise profile. This result highlights the NP's remarkable resistance to nonlinear spectral distortion. As for the USP, it exhibits extreme spectral broadening, shown in Figure 6(d) under 412 W operation, with SRS drastically reducing the SNR to just 7.3 dB. Critically, comparative analysis demonstrates that at 1 kW output power, the DPL exhibits significantly suppressed spectral broadening relative to the USP – an effect arising from the NP component, which endows the DPL with intermediate spectral characteristics between the NP and USP.

The pulse width of the NP measured by an oscilloscope is 0.44 ns at an output power of 1148 W, as illustrated in Figure 7(a). Meanwhile, the pulse width of the USP measured by an autocorrelator is 15.9 ps at an output power of 400 W, as shown in Figure 7(b). Under increasing output power, the NP demonstrates remarkable pulse width stability (0.42–0.44 ns), while the USP suffers from substantial pulse width broadening (5.6–15.9 ps).

The observed nonlinear effects originate mainly from the USP's high peak power in the fiber medium[26,27]. The pulse width of the NP (0.44 ns) is approximately 27 times that of the USP (15.9 ps), leading to a proportional reduction in peak

https://doi.org/10.1017/hpl.2025.10088 Published online by Cambridge University Press

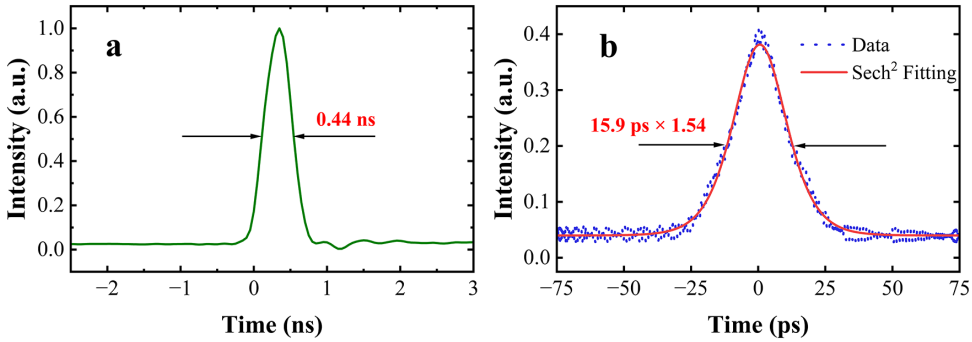


Figure 7. (a) Pulse width of the NP recorded using an oscilloscope. (b) Autocorrelation trace of the amplified USP.

Table 1. Amplification characteristics under varying temporal intervals.

Temporal interval (ns)	Repetition rate (MHz)	Output power (W)	η (%)	SNR (dB)
4.2	16	1092	80.0	22.0
	3.2	708	69.3	26.5
–1.5	16	1089	79.6	20.8
	3.2	714	69.9	24.4

power. Thus, it demonstrates that spectral broadening in DPL amplification is primarily governed by the USP component. Furthermore, the broadened DPL spectrum adversely affects amplifier efficiency through nonlinear processes. Spectral broadening triggers rapid nonlinear accumulation, leading to irreversible energy transfer to Raman-shifted wavelengths. This cascade effect ultimately causes signal depletion and degraded pump-to-signal conversion efficiency.

3.2.1. Impact of temporal intervals on optical amplification characteristics

To systematically investigate the influence of temporal intervals on amplification dynamics, the temporal intervals are set to 4.2 and –1.5 ns. As shown in Table 1, at temporal intervals of 4.2 and –1.5 ns, the maximum output powers at a repetition rate of 16 MHz are 1092 and 1089 W, with corresponding η of 80.0% and 79.6%, and spectral SNRs of 22.0 and 20.8 dB, respectively, demonstrating nearly identical amplification performance. Similar amplification characteristics are also observed at a repetition rate of 3.2 MHz.

Owing to the limited temporal resolution of the current detection system, the minimum temporal interval is controlled at 1.5 ns. Consequently, the above conclusion is strictly valid only for temporal intervals exceeding 1.5 ns. However, as temporal intervals decrease into the ps and sub-ns regime, significant nonlinear inter-pulse interactions are expected to emerge, fundamentally altering the amplification dynamics[28]. Specifically, theoretical studies indicate that a diminishing temporal interval between pulses can lead to pronounced competitive energy extraction mediated by gain and loss dynamics[29]. Therefore, elucidating the underlying physical principles of this competitive extraction mechanism warrants further investigation to optimize the performance of USP amplification systems.

3.2.2. Amplification characteristics under low-repetition-rate operation

In response to industrial demands for enhanced performance, this study investigates the DPL amplification at 6.4 and 3.2 MHz repetition rates, which support high-energy pulses. Figure 8 presents the output power, spectra and temporal

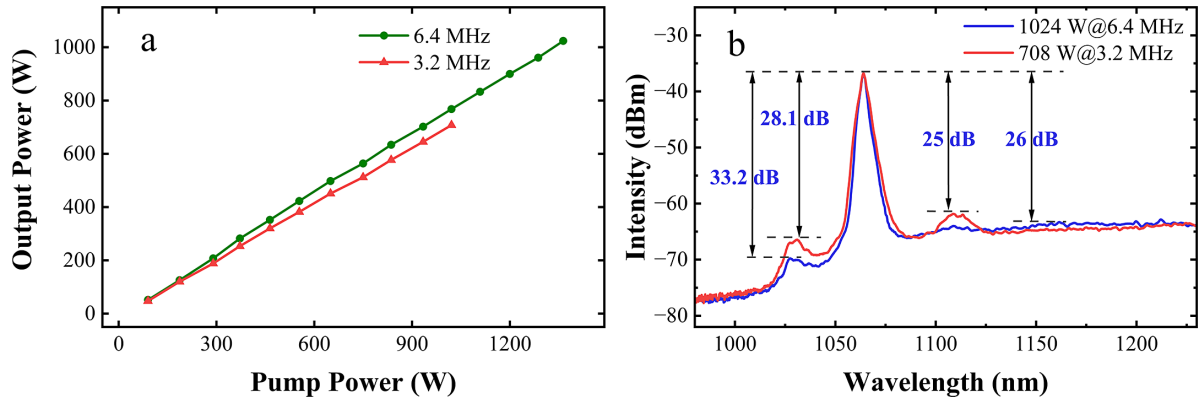


Figure 8. (a) The output power of the DPL and (b) the amplified spectra of the DPL at 6.4 and 3.2 MHz.

https://doi.org/10.1017/hpl.2025.10088 Published online by Cambridge University Press

profiles of the DPL. At 6.4 MHz, the system achieves a maximum output power of 1024 W ($\eta = 75.1\%$) with a spectral SNR of 26 dB, while at 3.2 MHz, the maximum power reaches 708 W ($\eta = 69.3\%$) with an SNR of 25 dB, as shown in Figures 8(a) and 8(b). The maximum pulse energy of the DPL is 221 μJ (3.2 MHz@708 W). Meanwhile, Figure 8(a) reveals a linear dependence between the DPL output power and pump power under both repetition rate conditions.

As demonstrated in Figure 8(b), the measured spectral SNRs exhibit distinct dependencies on repetition rate and output power. At 6.4 MHz with 1024 W output power, the SNR is quantified as 33.2 dB for ASE and 26 dB for SRS. When operating at 3.2 MHz with 708 W output power, the corresponding SNR decreases to 28.1 dB (ASE) and 25 dB (SRS), respectively. This systematic characterization reveals that lower repetition rates significantly promote ASE generation, as evidenced by the SNR reduction[30]. This behavior can be attributed to the reduced energy extraction efficiency under low-repetition-rate operation, which creates favorable conditions for ASE development.

4. Conclusion

This study presents an all-fiber DPL system capable of high-power, temporally adjustable optical pulses. Based on a flexibly tunable DPL generator with independent temporal modulation, DPLs with pulse widths of 5.6 ps and 0.42 ns are successfully achieved, wherein the temporal interval and the power ratio can be continuously adjusted. Meanwhile, the repetition rate can be continuously tuned over a range from 100 kHz to 32 MHz. Furthermore, analysis of various pulse combinations reveals two critical amplification characteristics: (1) the temporal interval (>1.5 ns) exhibits negligible influence on DPL amplification; (2) the amplified power ratio exhibits nonlinear variation due to component-dependent nonlinear effects, and SRS correlates specifically with pulse peak power. The DPL power ratio remains stable during amplification at pulse energies of less than 7.75 μJ (124 W@16 MHz), indicating excellent power-independent control. Using the MOPA configuration, the system achieves a maximum output power of 1092 W at 16 MHz. At 3.2 MHz, the pulse energy of the DPL reaches up to 221 μJ, with the respective pulse widths of 15.9 ps and 0.44 ns. The high-power DPL system represents a paradigm-shifting advancement, combining programmable ps-ns pulse coordination, nonlinear-effect-mitigated kW operation and simultaneous precision-energy delivery, establishing a transformative platform for next-generation scientific and industrial laser applications.

Acknowledgements

This work was financially supported by the National Key R&D Program of China (Grant Nos. 2022YFB3607800 and 2023YFB4604501), the CAS Project for Young Scientists in Basic Research (Grant No. YSBR-065), the National Natural Science Foundation of China (Grant Nos. 62225507, 62175230, 62175232, 62475254 and 62275244) and the Beijing Municipal Science & Technology Commission (Grant No. Z231100006023010).

References

1. I. Coddington, N. Newbury, and W. Swann, Optica **3**, 414 (2016).
2. F. R. Giorgetta, W. C. Swann, L. C. Sinclair, E. Baumann, I. Coddington, and N. R. Newbury, Nat. Photonics **7**, 435 (2013).
3. H. Bergeron, L. C. Sinclair, W. C. Swann, C. W. Nelson, J.-D. Deschênes, E. Baumann, F. R. Giorgetta, I. Coddington, and N. R. Newbury, Optica **3**, 441 (2016).
4. E. Baumann, F. R. Giorgetta, W. C. Swann, A. M. Zolot, I. Coddington, and N. R. Newbury, Phys. Rev. A **84**, 062513 (2011).
5. I. Coddington, W. C. Swann, L. Nenadovic, and N. R. Newbury, Nat. Photonics **3**, 351 (2009).
6. V. Z. Yuan Lu, X. Mao, R. Zheng, and R. E. Russo, J. Anal. At. Spectrom. **28**, 743 (2013).
7. C. Kerse, H. Kalaycıoğlu, P. Elahi, B. Çetin, D. K. Kesim, Ö. Akçaalan, S. Yavaş, M. D. Aşık, B. Öktem, and H. Hoogland, Nature **537**, 84 (2016).
8. P.-H. Wu, H.-T. Young, and K.-M. Li, Appl. Phys. A Mater. Sci. Process. **128**, 450 (2022).
9. T. Mizuno, Y. Nakajima, Y. Hata, T. Tsuda, A. Asahara, T. Kato, T. Minamikawa, T. Yasui, and K. Minoshima, Opt. Express **29**, 5018 (2021).
10. B. Li, J. Xing, D. Kwon, Y. Xie, N. Prakash, J. Kim, and S.-W. Huang, Optica **7**, 961 (2020).
11. Y. Nakajima, Y. Kusumi, and K. Minoshima, Opt. Lett. **46**, 5401 (2021).
12. S. Yang, C. R. Smith, C. R. Petersen, and O. Bang, Laser Photonics Rev. **19**, 2500074 (2025).
13. A. R. Cuevas, H. J. Kbashi, D. Stoliarov, and S. Sergeyev, Results Phys. **46**, 106260 (2023).
14. Y. Qin, B. Cromey, O. Batjargal, and K. Kieu, Opt. Lett. **46**, 146 (2021).
15. S. Galtier, C. Pivard, J. Morville, and P. Rairoux, Opt. Express **30**, 21148 (2022).
16. M. Kowalczyk, Ł. Sterczewski, X. Zhang, V. Petrov, Z. Wang, and J. Sotor, Laser Photonics Rev. **15**, 2000441 (2021).
17. K. Fritsch, T. Hofer, J. Brons, M. Iandulskii, K. F. Mak, Z. Chen, N. Picqué, and O. Pronin, Nat. Commun. **13**, 2584 (2022).
18. J. Pupeikis, B. Willenberg, S. L. Camenzind, A. Benayad, P. Camy, C. R. Phillips, and U. Keller, Optica **9**, 713 (2022).
19. N. Modsching, J. Drs, P. Brochard, J. Fischer, S. Schilt, V. J. Wittwer, and T. Südmeyer, Opt. Express **29**, 15104 (2021).
20. R. Kashyap, *Fiber Bragg Gratings*, 2nd edn (Academic Press, 2010).
21. R. Ahmed, J. Iqbal, and M. A. Baig, Laser Phys. Lett. **12**, 066102 (2015).
22. L. Yang, J. Wei, Z. Ma, P. Song, J. Ma, Y. Zhao, Z. Huang, M. Zhang, F. Yang, and X. Wang, Nanomaterials **9**, 1789 (2019).
23. C. Ning, S. Zou, H. Yu, J. Zuo, X. Chen, S. Xu, S. Han, X. Li, W. Wu, C. He, and X. Lin, High Power Laser Sci. Eng. **11**, e88 (2023).
24. J. Zuo, H. Yu, S. Zou, Z. Dong, C. He, S. Xu, C. Ning, X. Chen, X. Li, and X. Lin, High Power Laser Sci. Eng. **11**, e22 (2023).

https://doi.org/10.1017/hpl.2025.10088 Published online by Cambridge University Press

25. X. Li, H. Yu, S. Zou, C. He, C. Ning, W. Wu, X. Chen, and X. Lin, High Power Laser Sci. Eng. **12**, e87 (2024).
26. X. Dai, Y. Qi, Q. Yu, C. He, S. Yang, and Z. Lu, Chaos, Solitons Fractals **197**, 116506 (2025).
27. Y. Qi, Y. Gao, T. Zhang, C. He, Z. Lu, D. Yan, W. Sun, X. Lin, and S. Yang, J. Lightwave Technol. **43**, 4000 (2025).
28. Y. Qi, W. Wang, Z. Wang, Y. Gao, Z. Zhu, C. He, Z. Lv, S. Yang, and X. Lin, Opt. Express **33**, 516 (2025).
29. X. Chen, W. Lin, X. Hu, W. Wang, Z. Liang, L. Ling, Y. Yang, Y. Guo, T. Liu, D. Chen, X. Wei, and Z. Yang, Light Sci. Appl. **13**, 265 (2024).
30. J. C. Zheng, J. Y. Xie, Q. Q. Liu, C. J. He, Y. Y. Qi, L. Li, L. H. He, C. B. Liu, X. C. Lin, and S. Yang, Appl. Phys. Lett. **125**, 051106 (2024).

https://doi.org/10.1017/hpl.2025.10088 Published online by Cambridge University Press